A Miniaturized Integrated Rectenna Sensor System for Simultaneous Energy Harvesting and Data Transfer

Journal:	*IEEE Sensors Journal*
Manuscript ID	Sensors-62280-2023
Manuscript Type:	Regular Paper
Date Submitted by the Author:	26-Jul-2023
Complete List of Authors:	Kumar, Sundeep; Indian Institute of Technology Ropar, Electrical Engineering Kumar, Manoj; Indian Institute of Technology Ropar, Electrical Engineering Sharma, Ashwani ; Indian Institute of Technology Ropar, Electrical Engineering
Keywords:	APPL

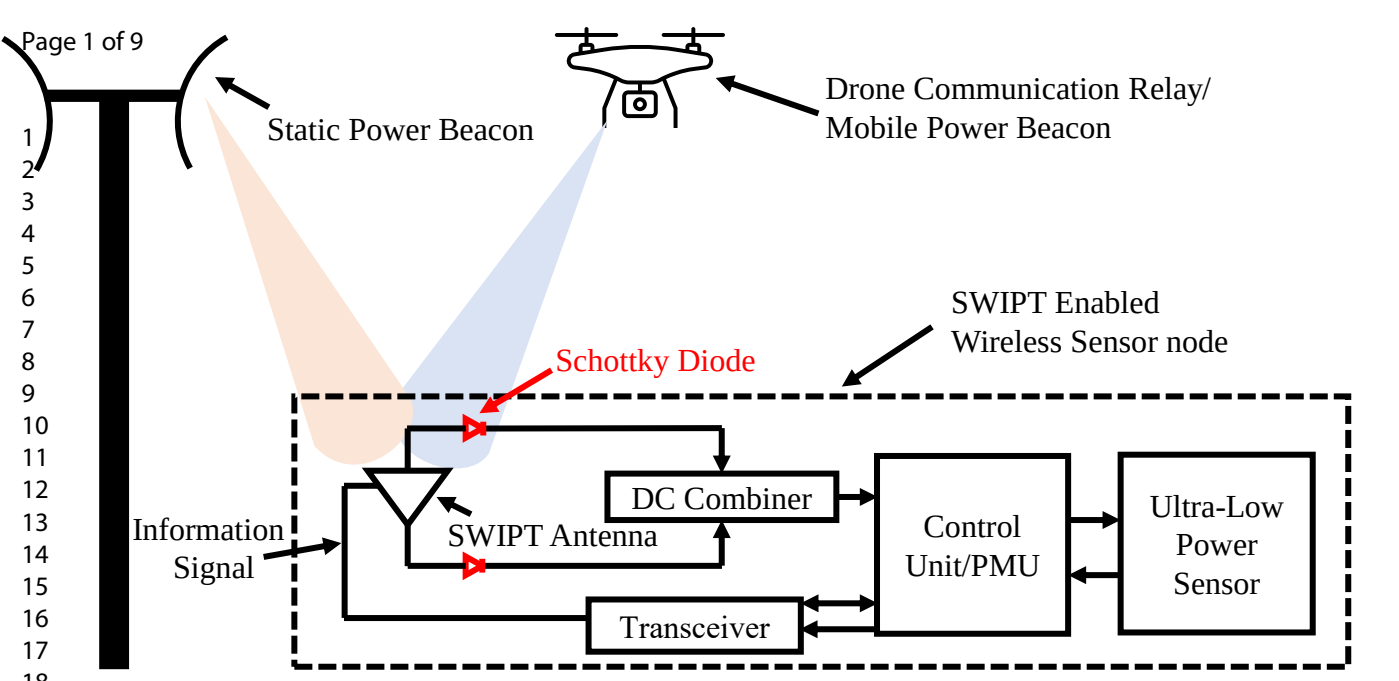
Static Power Beacon
Drone Communication Relay/
Mobile Power Beacon
SWIPT Enabled
Wireless Sensor node
Schottky Diode
DC Combiner
SWIPT Antenna
Information
Signal
Control
Unit/PMU
Ultra-Low
Power
Sensor
Transceiver

IEEE Sensors Council IEEE SENSORS JOURNAL, VOL. XX, NO. XX, XXXX 2017 1

A Miniaturized Integrated Rectenna Sensor System for Simultaneous Energy Harvesting and Data Transfer

Sundeep Kumar, *Graduate Student Member, IEEE*, Manoj Kumar, *Member, IEEE*, and Ashwani Sharma, *Senior Member, IEEE*

***Abstract*— Wireless sensor networks (WSN) have a short lifetime due to the limited battery capacity of IoT sensor nodes, which reduces network sustainability and increases maintenance cost. To address this issue, a dual-band three-port SWIPT antenna system is proposed to concurrently recharge sensor node batteries and facilitate wireless information transfer (WIT). The two co-polarized wireless power transfer (WPT) ports are conjugate impedance matched with a series Schottky diode and the resulting dc outputs are further combined in parallel to realize an ultra-low power full-wave rectenna system. The cross-polarized proximity-fed WIT port and capacitively coupled WPT ports are utilized to achieve high port isolation. The proposed feeding mechanism inhibits information signal leakage into the rectenna (≤ -21.5 dB), and impedes dc backflow into the WIT port. Moreover, it maintains a high radiation efficiency of around 80%. Further, the proposed system is fully integrated to achieve miniaturization, making it suitable for small sensor nodes in WSN applications.**

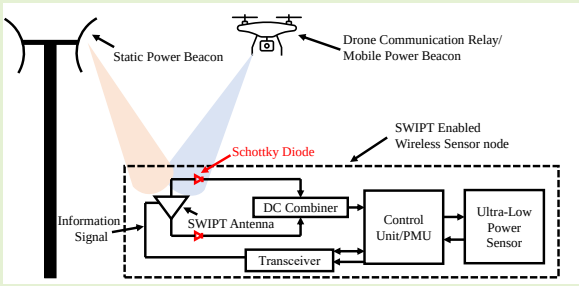

***Index Terms*— Energy harvesting, wireless power transfer, wireless information transfer, full-wave rectenna, IoT, SWIPT, microstrip antennas**

I. Introduction

THE future 6G communication networks will witness the deployment of a large number of sensor nodes to realize smart applications [1]. Many energy harvesting (EH) schemes are investigated in the literature to enhance the lifespan of the sensor nodes. The wireless power transfer (WPT) technology has emerged as the most popular choice [2], [3] as it provides easy integration with the existing communication circuitry. Moreover, the sensor nodes collect information related to the surrounding environment and communicate it with a remote gateway through a wireless information transfer (WIT) antenna. However, employing two separate antenna modules for WPT and WIT results in a bulky sensor node. To address this problem, several research works have recently been reported towards implementing simultaneous wireless information and power transmission (SWIPT) to achieve concurrent data and power transfer to remote sensor nodes [4].

To realize SWIPT operation, several existing schemes can be employed, such as power splitting [5]–[7], time splitting [5], dual polarization [8], [9], frequency splitting [10], and space splitting [11], [12], as depicted in Fig. 1. The power-splitting technique divides the received signal into two power ratios for information decoding and RF power harvesting, as shown in Fig. 1(a). However, this reduces the signal-to-noise ratio (SNR) as well as the power conversion efficiency

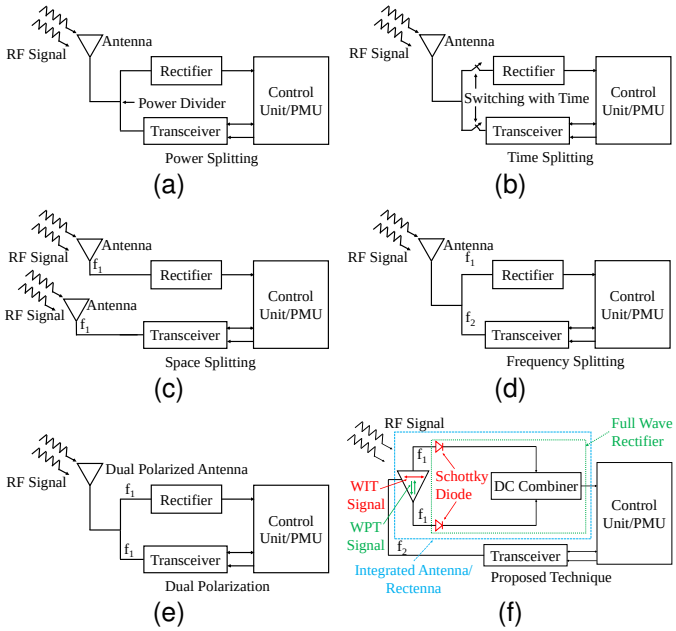

Fig. 1. (a)-(e) Various SWIPT Techniques proposed in the existing literature (f) proposed integrated SWIPT technique

This work was supported in part by SERB, Department of Science & Technology, Government of India under Grant CRG/2022/007257.

Authors are with Electrical Engineering department, Indian Institute of Technology Ropar, Punjab, India. (E-mail: sundeep.19eez0004@iitrpr.ac.in, 2018eez0020@iitrpr.ac.in, ashwani.sharma@iitrpr.ac.in).

(PCE) of the rectifier circuit. In contrast, the time-splitting technique depicted in Fig. 1(b) provides enough RF signal power for acceptable SNR and PCE since different time slots are used for information and power transmission. However, the major drawback of this scheme is the requirement of time-synchronization between the transmitter and the receiver [13]. Moreover, the optimal time divisions for various sensor nodes are different to achieve sustainable IoT operation. On the other hand, the space-splitting scheme, exemplified in Fig. 1(c) employs separate antenna elements for WIT and WPT operations at the same frequency. In contrast, the frequency splitting technique utilizes different frequency channels for information and power transfer [10], [14], [15], as demonstrated in Fig. 1(d) whereas, in dual-polarization [8], [9], [16] technique cross-polarized ports are employed at the same frequency, as exhibited in Fig. 1(e). Further, a few hybrid SWIPT antenna systems are reported in the literature. For instance, a shared aperture antenna [17] with frequency splitting, a dual-polarized full-duplex antenna [18], [19], and a frequency splitting with dual-polarization [14] are proposed. However, these designs either use multiple antenna elements [17]–[19] or rectifier impedance matching network [14], which results in a bulky antenna system making them unsuitable for small sensor nodes. In contrast, the frequency splitting and dual-polarization methods are relatively less complicated to implement as they employ distinct frequency channels and orthogonal polarization for the transmission of data and power, respectively. This enables high isolation between the WIT and WPT ports, resulting in improved SNR and PCE of the SWIPT antenna. In existing SWIPT systems, antenna and rectifier circuit are matched either using the impedance matching network (IMN) [14], [15] or employing loop-based conjugate matching techniques [8], [10], [16]. However, loop-based conjugate matching technique requires partial ground structure which suffers from variation in antenna characteristics [20] when the IoT sensor node is placed over different platforms having different dielectric properties. In addition, the existing conjugate-matched SWIPT antennas [8], [16] employ voltage doubler topology to realize full-wave rectification (FWR) for achieving enhanced PCE ($\sim 70\%$) at high input RF power (≥ 500 μW) [21]. However, realizing FWR for ultra-low power (-10 dBm) [22] applications with such a high PCE poses a significant challenge [10]. Moreover, ultra-low power RF transmission is desired in IoT applications where human presence is warranted to satisfy the SAR limit of 1.6 W/kg and protect human tissues from any damage. Therefore, a miniaturized robust antenna having high WIT radiation efficiency and high PCE for ultra-low power WPT is desired for SWIPT applications. This paper presents a novel miniaturized SWIPT antenna system utilizing the integration of frequency splitting and dual polarization techniques as demonstrated in Fig. 1(f). Moreover, this is the first attempt to design an integrated antenna and DC-combined, ultra-low power FWR for SWIPT-enabled sensor nodes. The major contributions of the proposed work are the following:

- The proposed design comprises two co-polarized WPT ports for harvesting subsequent half cycles of the ultra low power RF waves incident on the antenna aperture,
- The series Schottky diode connection topology is utilized at WPT ports. The corresponding dc outputs are then combined in parallel for realizing inherent FWR to deliver significant efficiency improvement over half-wave rectification (HWR) for ultra-low power incident RF waves,
- The cross-polarized proximity-fed WIT port and capacitively coupled WPT ports are employed to achieve high port isolation with the ability to impede dc backflow into the antenna and WIT port,
- The proposed feeding mechanism enables the realization of integrated conjugate impedance matching with the rectifier circuit. In addition, the integrated FWR realizes high radiation efficiency and PCE for WIT and WPT respectively, resulting in efficient simultaneous data and power transfer with a compact antenna footprint.

This work is divided into five sections. Section II presents the system architecture of the proposed SWIPT antenna system along with the application scenario. The evolution of the proposed antenna is discussed in Section II-C. The simulation conditions and results of the final design are analyzed in II-D. The experimental setup and measurement results are discussed in Section III to validate the simulation results. Section IV presents the comparison of the proposed antenna with the state-of-the-art designs. The relevance of the proposed work for achieving sustainable sensors is discussed in Section V. The paper is concluded in Section VI.

II. Proposed SWIPT Antenna Design and Simulation

A. System Architecture

The SWIPT antenna is essential for data communication and RF power harvesting, therefore, the antenna design procedure is bifurcated into two steps. The first step describes a 50 Ω antenna design for WIT at 5.8 GHz (5.7 GHz - 6 GHz) to cater data communication in the upper 5 GHz WiFi and vehicular communication band [23], with a bore-sight radiation pattern. In the next step, a direct conjugate-matched, dc-combined, fully-integrated rectenna is evolved within the same design for WPT with maximum PCE at 5.2 GHz. In general, a lower frequency is chosen for WPT to achieve a larger transmission range [10]. The 5.2 GHz frequency channel is in the lower 5 GHz WiFi band (5.15 GHz - 5.35 GHz). In addition, high isolation is required between the WIT and WPT signals in the SWIPT antenna since the information signal can leak power into the rectifier circuit due to mutual coupling. Thus, low isolation will reduce the information signal strength, resulting in low communication link quality. The application scenario for the proposed antenna is illustrated in abstract figure. A SWIPT-enabled IoT sensor node can communicate the sensed data either directly with a remote gateway or through a mobile drone communication relay. Additionally, sensor nodes can harvest RF power from a locally installed static or mobile drone power beacon. These sensor nodes facilitate the implementation of various IoT applications, including smart homes, smart warehouses, smart farming, smart transportation, etc.

TABLE I
DIMENSIONS OF THE PROPOSED SWIPT ANTENNA.

Parameters	W_1	W_2	W_3	W_4	W_5	W_6	L_1	L_2	L_3	L_4	L_5	L_6	L_7	L_8	L_9	L_{10}	L_{11}	L_{12}	D	d	g_p
Dimension (mm)	3	1	0.55	0.35	0.55	1.1	11	1.6	5.43	1.37	10.52	9.9	21.25	2	2	30	23.45	27.45	12.2	0.5	0.6

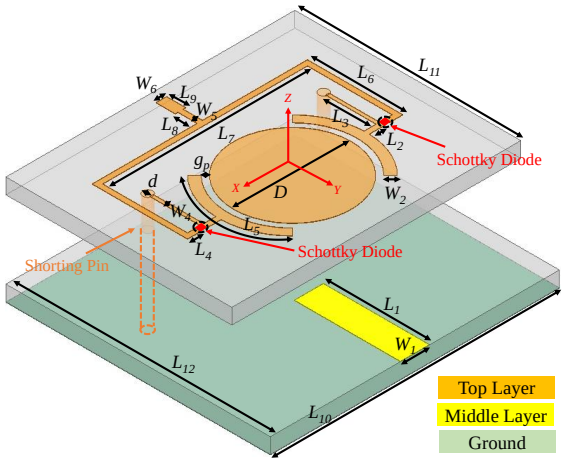

Fig. 2. Exploded view of the proposed simulated SWIPT antenna design.

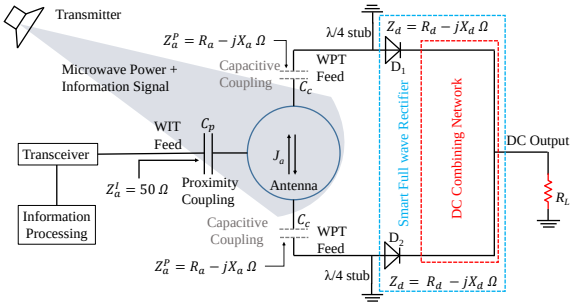

Fig. 3. Equivalent circuit diagram of the proposed SWIPT antenna.

B. Design and Layout

The proposed antenna is designed using Ansys HFSS on FR4 substrate ($\epsilon_r = 4.4, \tan\delta = 0.02$) having 1.6 mm thickness with 35 μm copper cladding. The rectifier circuit analysis is carried out using harmonic balance (HB) simulation in advanced design system (ADS) software and the final design layout is demonstrated in Fig. 2, indicating various design parameters listed in Table I.

The equivalent circuit diagram of the proposed SWIPT antenna is shown in Fig. 3 to explain its working mechanism. The capacitor C_p represents the proximity coupled WIT feed with $Z_a^I = 50\Omega$ input port impedance which can be further connected to the transceiver module for communication. The two capacitively coupled co-polarized WPT feed lines are depicted by capacitors C_c with an input port impedance ($Z_a^p = R_a - jX_a\ \Omega$) conjugate matched to the Schottky diode impedance ($Z_d = R_d + jX_d\ \Omega$). The low-pass filter characteristics of the central patch antenna [24], and the capacitively coupled WPT feed inhibits dc backflow and facilitates the inherent integration of the rectifier circuit and antenna. Moreover, the WPT feed lines are orthogonal to WIT feed to achieve high isolation between information and power signals. The RF waves impinging on the circular patch generate TM_{110} mode current (J_a) on the antenna surface.

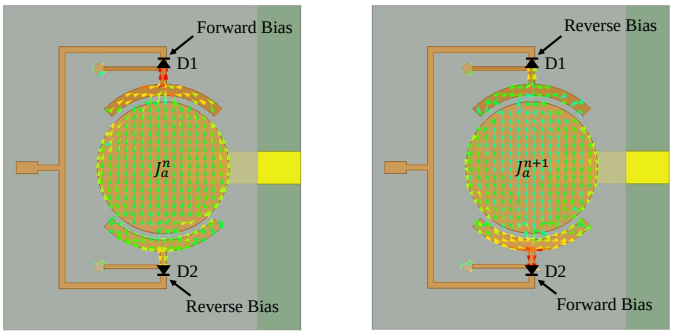

Fig. 4. Current distribution on the proposed antenna when (a) Diode D1, and (b) Diode D2 is forward biased.

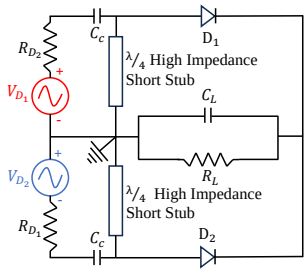

Fig. 5. Working Principle of RF signal rectification in the proposed SWIPT antenna.

The current direction changes in each subsequent half cycle of the incident RF wave and is illustrated in Fig. 3 with two arrows directed towards the opposite direction. Therefore, to convert the RF power captured in each half cycle into usable dc power the two diodes are connected in mirror symmetry (anode terminal of diode connected to patch) with respect to the patch center.

The surface current distribution in the proposed antenna for diode D_1 and D_2 excitation are illustrated in Fig. 4 (a) and (b), respectively. Additionally, the working principle of the proposed rectification circuit is depicted by voltage sources V_{D1-D2} having an internal impedance of R_{D1-D2}, as demonstrated in Fig. 5. The surface current excited (J_a^n) in patch antenna during n^{th} half cycle of incident RF wave forward bias Schottky diode D_1. In the next $(n+1^{th})$ half cycle, the surface current (J_a^{n+1}) flows in reverse direction to J_a^n, forward biasing Schottky diode D_2. In reverse bias conditions, the Schottky diode does not contribute to the dc output and act as an open load. Further, the cathode terminals of both the diodes are joined together through dc connection lines to combine output dc voltage in subsequent half cycles. The second dc terminal is extracted at the ground using a $\lambda/4$ short stub connected to the anode terminals of the Schottky diodes. The short stub provides necessary isolation between the RF signal and dc output as well as suppresses even order harmonics generated by the Schottky diodes [25]. Overall in the proposed circuit, each Schottky diode behaves as HWR and the parallel combination of the

two achieves an integrated FWR system [26]. The parallel combining discussed in the literature combines the dc output of two separate antenna elements. In contrast, the proposed parallel dc combining topology fuses the dc outputs from two co-polarized ports of the same antenna activated in subsequent half cycles of incident RF wave behaving in itself as a smart FWR. The proposed SWIPT antenna is carefully designed through a step-by-step process to ensure optimal performance in terms of radiation efficiency, power conversion efficiency, and impedance matching. A detailed explanation of the evolution of the proposed SWIPT antenna is discussed in the subsequent subsection.

C. Design Evolution

The detailed design evolution of the proposed SWIPT antenna is illustrated in Fig. 6. The proposed antenna is a three-

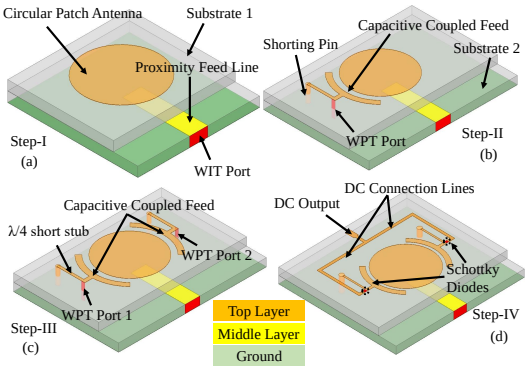

Fig. 6. Design evolution of the proposed SWIPT antenna.

layer structure implemented using two FR4 substrates (substrate 1 and substrate 2). Moreover, a circular patch is chosen for designing the SWIPT antenna system as it possesses the natural ability to reject harmonics (nf_0, $n \in \mathbb{N}$) generated by Schottky diode since it resonates at frequencies that are non-integer ($n \notin \mathbb{N}$) order [27] of the fundamental frequency. First, the patch is excited with a proximity-coupled feed line for WIT as illustrated in Fig. 6(a). The antenna design parameters are optimized to achieve the desired impedance (Z_a^I) bandwidth (5.7 GHz-6 GHz) and is demonstrated by S_{11} plots in Fig. 7 (a) for each evolution step. In the second step, a capacitively

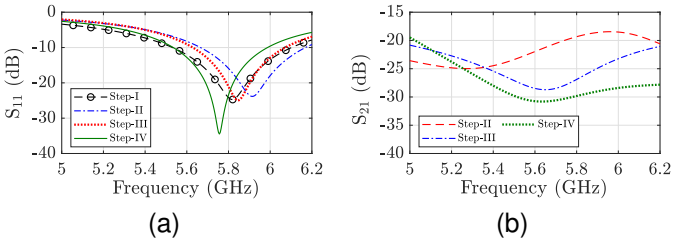

Fig. 7. (a) Simulated reflection coefficient ($\mathbf{S_{11}}$) of the WIT Port, and (b) Isolation ($\mathbf{S_{21}}$) between the WIT and WPT ports at various design evolution stages of the proposed SWIPT antenna.

coupled WPT feed is implemented in cross-polarization with WIT feed, as shown in Fig. 6(c). The cross-polarized WPT and WIT feeds achieve high isolation between information and power signals as indicated by S_{21} plots in Fig. 7 (b). Moreover, the capacitive coupling inhibits dc back-flow into the antenna [28] and also enables conjugate impedance matching between the antenna (Z_a^P) and the rectifier circuit (Z_d) at 5.2 GHz with a small footprint. A $\lambda/4$ high impedance short stub is employed to block RF signal flow into the ground and provide dc connection to the load [29]. The SMS-7621−079LF Schottky diode is utilized to execute the rectification operation due to its low junction capacitance, high cutoff frequency, and excellent power threshold efficiency for low input RF power range [30]. The input impedance ($Z_d = 25 - j75\ \Omega$) of the Schottky diode is evaluated using ADS for an input RF power of −10 dBm. The 1 kΩ resistance is taken as reference load to conjugate match the antenna impedance with the Schottky diode impedance [26]. Similarly, in the subsequent step shown

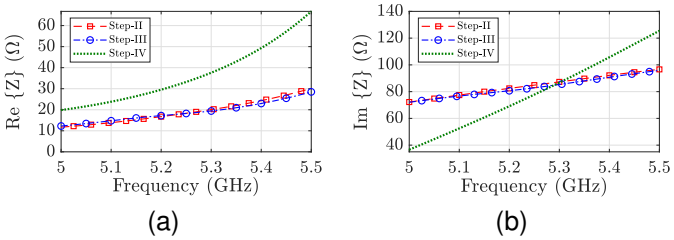

Fig. 8. (a) Real, and (b) Imaginary part of the WPT port input impedance at various design evolution stages of the proposed SWIPT antenna.

in Fig. 6 (c), a second co-polarized WPT port 2 is realized by connecting the Schottky diode in mirror symmetry to the one connected to WPT port 1. In the final step, the dc outputs from both WPT ports 1 and 2 are parallel combined, as demonstrated in Fig. 6 (d), to achieve inherent FWR, as described in section II-B. Moreover, the combining circuit assists in achieving improved direct impedance matching with the rectifier circuit, as depicted in Fig. 8 (a) and Fig. 8 (b). In addition, the intended WIT impedance bandwidth mentioned earlier is also achieved, with high isolation between WIT and WPT ports for the proposed antenna as illustrated by step-IV plots in Fig. 7 (a) and Fig. 7 (b), respectively.

D. Simulation Results and Discussion

The simulated S_{11} of WIT port illustrated in Fig. 7 (a) indicates the antenna impedance bandwidth ($S_{11} < -10$) of 5.53 GHz - 6.0 GHz. In addition, the input impedance of the power port $(29.67 + j69.43)\ \Omega$ is optimized by changing antenna parameters to achieve conjugate impedance matching with rectifier circuit impedance $(25 - j75)\ \Omega$. Moreover, the simulated isolation (S_{21}) between the WIT and WPT port is greater than 28 dB for the entire WIT band of operation, i.e., 5.7 GHz - 6 GHz. This inhibits the leakage of information signal into the rectifier circuit and hence maintains the required communication link quality in terms of SNR. The simulated normalized RF radiation patterns of the antenna and rectenna functions are depicted in Fig. 9 (a) and Fig. 9 (b), respectively. The results indicate boresight RF radiation patterns for WPT and WIT operations. Moreover, the realized RF radiation gain for the antenna and rectenna is 5.7 dBi and 3.65 dBi, respectively. The $\phi = 0°$ and $\phi = 90°$ elevation plane patterns for the proposed antenna have 3 dB beamwidth of 84° and 92°, respectively. Similarly, the rectenna has 3 dB

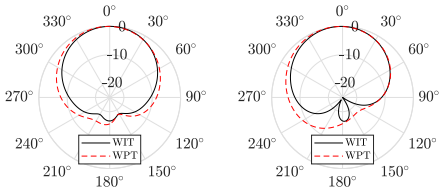

Fig. 9. Simulated normalized RF radiation pattern of information and power signal in (a) $\phi = \mathbf{0}°$, and (b) $\phi = \mathbf{90}°$ elevation plane at $\mathbf{5.8}$ GHz and $\mathbf{5.2}$ GHz, respectively.

RF pattern beamwidth of $100°$ and $108°$ in $\phi = 0°$ and $\phi = 90°$ elevation planes. Further, the high radiation efficiency of 80.97% for rectenna operation is achieved at 5.2 GHz, and the same is $> 78\%$ for the antenna functioning in the operating communication band.

III. Antenna Fabrication and Measurement

A. Measurement Setup

The proposed SWIPT antenna is fabricated using the MITS PCB prototyping machine. The detailed description of the designed antenna prototype is demonstrated in Fig. 10. To

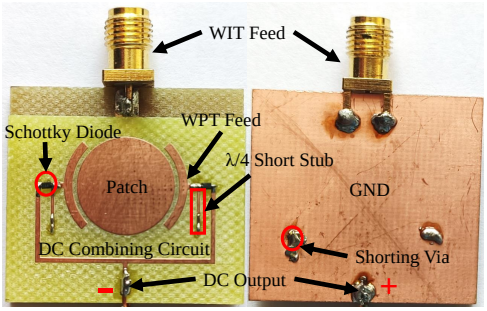

Fig. 10. Fabricated prototype of the proposed SWIPT antenna.

measure the WPT performance a horn antenna is used as the Tx and is fed by an RF signal generator. The proposed SWIPT antenna is mounted on the turn table and is placed at d distance from the Tx horn antenna. The received RF power at the antenna aperture is measured using a Keysight spectrum analyzer (N9951A), and the harvested dc voltage is measured across the dc output terminals of the rectenna using a Keysight multimeter (U1232A). The detailed description of the WPT transmitter link budget and propagation parameters utilized in the measurements are listed in Table II. In contrast,

TABLE II
Link Budget Parameters

WPT Transmitter and Propagation Parameters	
Frequency (f)	5.2 GHz
Signal generator power (P_t)	25 dBm
Measured Cable Loss L_c	2.3 dB
Transmitter antenna (horn) gain (G_t)	10.5 dBi
EIRP ($P_t + G_t - L_c$)	33.2 dBm
Distance (d)	1 m

the information signal performance is measured using the Keysight PNA-L (N5234B) VNA. The measurement of WIT signal radiation pattern and the harvested dc power pattern at

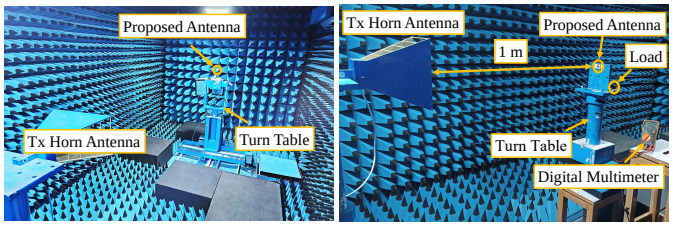

Fig. 11. Experimental setup to measure (a) Antenna RF radiation pattern, and (b) Rectenna DC power pattern and PCE.

the WPT port is carried out in the anechoic chamber using the experimental setup illustrated in Fig. 11 (a) and Fig. 11 (b), respectively.

B. Measurement Results and Discussion

1) Impdeance matching and Pattern measurements: The reflection coefficient of the WIT port is measured by using Keysight PNA-L and is demonstrated in Fig. 12. The results

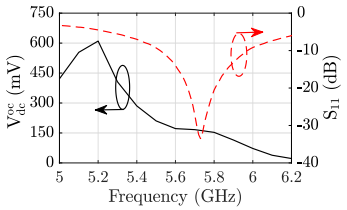

Fig. 12. Measured WIT port reflection coefficient and the output open dc voltage of the proposed SWIPT antenna.

indicate that the impedance bandwidth ($S_{11} \leq -10$ dB) of the proposed SWIPT antenna is 5.7 GHz - 6.0 GHz. Although the measured bandwidth exhibits slight deviations from the simulation results, but it does not negatively impact the performance of the upper 5 GHz WiFi or vehicular communication channels. The impedance matching of the WPT port cannot be measured using VNA due to the conjugate matching. Therefore, harvested open dc voltage is plotted in Fig.12 for signals ranging from 5 GHz-6.4 GHz. The results show maximum output open dc volage of 610.2 mV, indicating impedance matching of the WPT ports at 5.2 GHz. The measured information signal RF radiation patterns are

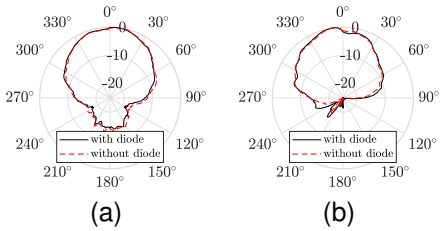

Fig. 13. Measured RF radiation pattern of the WIT signal in (a) $\phi = \mathbf{0}°$, and (b) $\phi = \mathbf{90}°$ elevation plane at $\mathbf{5.8}$ GHz with and without Schottky diode.

exhibited in Fig. 13. The results indicate a very insignificant effect of the Schottky diode on RF radiation pattern, and gain of 5.65 dBi and 5.57 dBi is noted with and without the rectifier circuit. Moreover, the measured $\phi = 0°$ and $\phi = 90°$ elevation plane RF patterns for WIT signal have 3 dB beamwidth of $66.7°$ and $75.6°$, respectively. The deviation of the measured

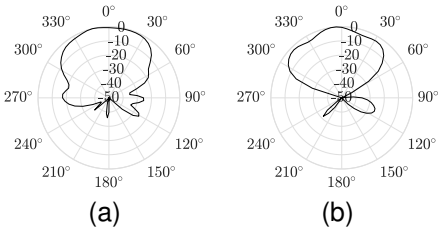

Fig. 14. Measured normalized output dc power pattern of WPT in (a) $\phi = \mathbf{0}°$, and (b) $\phi = \mathbf{90}°$ elevation plane at $\mathbf{5.2}$ GHz.

values from the simulated results can be attributed to the non-ideal dielectric material and fabrication errors. Further, the dc power pattern of the rectenna shown in Fig. 14, indicating close agreement with the simulated RF patterns plotted in Fig. 9.

2) PCE measurements: The harvested dc voltage and PCE of the rectenna are measured using the measurement setup shown in Fig. 11(b). The received RF power (P_r) is evaluated using the Friis transmission equation given in (1),

$$P_r(\text{dBm}) = \text{EIRP}(\text{dBm}) + G_r(\text{dBi}) + 20\log_{10}\left(\frac{\lambda}{4\pi d}\right) \quad (1)$$

where, G_r is the receiver realized gain, and λ is the RF signal wavelength. The evaluated P_r is later validated through measurement by the spectrum analyzer for complete characterization of the rectenna. The evaluated P_r for the proposed FWR operation is -9.91 dBm, and the results plotted in Fig. 15 indicate a maximum PCE of 66.52% with 203.5 mV output dc voltage at an optimal load of $610\ \Omega$. Moreover, one Schottky diode is removed to measure the PCE for HWR and determine the improvement achieved in PCE by the proposed FWR. Since the system is optimized for FWR, removing one diode resulted in a shift in impedance matching frequency to 5.56 GHz with simulated G_r of 5.44 dBi with evaluated $P_r = -8.7$ dBm. The results show a maximum PCE of 41.76% at $552.7\ \Omega$ load as demonstrated in Fig. 15 (a), indicating a

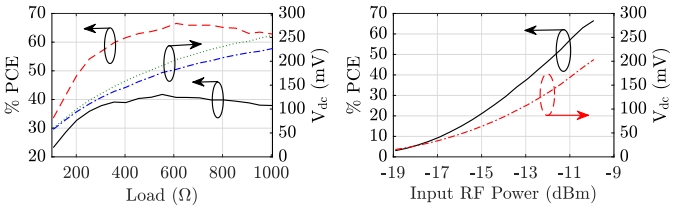

Fig. 15. (a) Measured PCE and harvested DC voltage vs Load of the proposed antenna for HWR at 5.56 GHz and FWR at 5.2 GHz, (b) PCE and harvested DC voltage vs input RF power at $\mathbf{610\ \Omega}$ output load at $\mathbf{5.2}$ GHz.

significant improvement in PCE due to the proposed FWR configuration. Further, change in PCE with respect to the variation in input RF power is measured and results are plotted in Fig. 15 (b). The measurement results show a non-linear increase in PCE and output dc voltage with respect to the input RF power corresponding to the non-linear $I-V$ characteristics of the Schottky diode.

3) Isolation measurements: The isolation between the WIT and WPT ports is validated using a two-step measurement process. In the first step, the proposed antenna is incident with a 5.7, 5.8, and 5.9 GHz RF signal using the measurement setup illustrated in Fig. 11 (b). The corresponding output open dc voltages ($V_{dc}^{oc} = 166.6, 153$, and 114.6 mV) are measured and the corresponding received RF power ($P_r = -8.81, -8.92$, and -9.2 dBm) at the antenna aperture are evaluated using (1). In the next step, the WIT feed of the proposed antenna is directly connected with the signal generator through an RF cable incurring $L_c = 1.6$ dB loss as shown in Fig. 16 (a). The RF power coupled to the WPT ports from the WIT

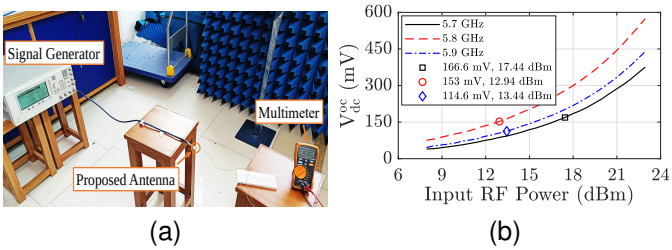

Fig. 16. (a) Experimental setup to measure isolation between WIT and WPT port of the proposed antenna, (b) Measured output open dc voltage vs RF power input to WIT feed.

port is converted to dc output by the Schottky diodes and is measured using a multimeter. The signal generator output power is varied from 10 dBm to 25 dBm effective input RF power ranging from 7.94 dB to 22.94 dB after considering cable and antenna reflection losses. The corresponding output open dc voltages are measured at different frequencies and are plotted in Fig. 16 (b). The results indicate 153 mV open dc voltage for 12.94 dBm RF input at 5.8 GHz, suggesting that -8.92 dBm power is coupled with the WPT ports, resulting in $12.94 + 8.92 = 21.86$ dB isolation between WIT and WPT ports. Similarly, the isolation at 5.7 GHz and 5.9 GHz evaluates to 26.25 dB and 21.64 dB, respectively. The measurement results show a close agreement with the simulated isolation results illustrated in Fig. 7 (b) and the small variations can be attributed to measurement and fabrication errors.

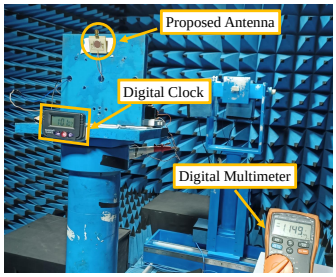

Fig. 17. Real-world demonstration of digital clock operation using proposed SWIPT antenna.

C. Real World Demonstration of Proposed SWIPT Antenna

A digital clock with voltage and current ratings of 1.1 V and $10\ \mu$A is integrated with the proposed antenna to demonstrate its real-world performance, as illustrated in Fig. 17. Since the voltage rating is higher than the open voltage (610.2 mV) of the proposed antenna, a series combination of four $470\ \mu$F capacitors is utilized to imitate dc-dc boost converter operation. First, each capacitor is charged individually and later

TABLE III
PERFORMANCE COMPARISON WITH STATE-OF-THE-ART

Parameters	[14]	[10]	[8]	[16]	[7]	[6]	[5]	This Work
Freq (GHz) WPT/WIT	5.8 / 6.1	0.868 / 2.4	2.4 / 2.4	2.4 / 2.4	5.8 / 5.8	5.2 & 5.73 / 5.2 & 5.73	2.4 / 2.4	5.2 / 5.8
Comms. gain (dBi)	7	7.2	5	8.4 - 9.6	4.71 – 5.15	4.22 – 5.68	3.64 – 4.10	5.7
Rectenna gain (dBi)	7.2	1.7	6.4	2.5 - 4	4.71 – 5.15	4.22 – 5.68	4.10 – 4.57	3.6
Total WIT Efficiency	NG	63%	41%	70% – 88%	NG	NG	90.5%	78% – 80.23%
Min. Port isolation (dB)	25	30	45	10 – 16	15	15	15	21.64
Received input Power (dBm)	13.97	−9.5	3	2	0.5	5	6	−9.91
Peak PCE	63%	63.9%	71%	70%	51.1%	50.2%	60.7%	66.52%
PCE @ −9.91 dBm	NG	60%	44%	55%	33%	≤ 30%	NG	66.52%
DC Combining	No	No	No	No	No	No	No	Yes
Direct Matching	No	Yes	Yes	Yes	No	No	No	Yes
Platform independent	Yes	No	No	No	No	No	No	Yes
SWIPT Technique employed	freq split + dual-pol	freq split	dual-pol	dual-pol	power split	power split	either power split or time split	freq split + dual-pol + dc combine
Rectification Topology	half wave	voltage doubler	voltage doubler	voltage doubler	half wave	half wave	half wave	full wave
Electrical size (λ_0 @ WIT freq)	$> 0.82 \times 1$	0.74×0.63	0.63×0.63	0.61×0.61	2.5×10.6	$> 1.57 \times 1.05$	$> 0.984 \times 0.432$	0.58×0.53

Abbreviations:- NG: not given; freq: frequency; pol: polarization; split: splitting

combined in series to operate the digital clock. The charging of each capacitor up to 500 mV requires 3 to 4 seconds, resulting in a total of $\sim$ 16 sec of charging time interval. The charged capacitors when connected in series are able to operate the clock for an interval of 20 sec. The immediately mentioned results indicate that the proposed antenna can operate small IoT sensor nodes after integration with an ultra-low power management unit housing a dc-dc boost converter.

IV. Performance Comparison

The performance of the proposed antenna is compared in Table III with the state-of-the-art SWIPT antennas. The designs in [10], [14] use frequency splitting for SWIPT operation, representing the most pertinent prior works for fair comparisons. The high port isolation ($\geq$ 25 dB) is achieved by utilizing cross-polarized ports in [14] and dual-mode operation in [10] for WIT and WPT functions. However, these antennas have lower PCE and WIT efficiency of about 63% as compared to the proposed design with PCE of 66.52% and WIT efficiency of 80%. Moreover, the matching network in [14] makes the design bulky. For instance, the proposed design is 34% and 62.51% miniaturized compared to the designs presented in [10], [14], respectively. In contrast to the immediately mentioned works, the antenna designs in [5]–[8], [16] deliver information and power at the same frequency. Here, dual-polarization [8], [16] and power splitting [5]–[7] techniques are employed to achieve the SWIPT operation. The linearly polarized design in [8] has cross-polarized WIT and WPT ports having high isolation of 45 dB but with lower WIT efficiency of 41% and low PCE of 43% at −10 dBm input RF power. Similarly, in [16], cross-polarized ports are used with dual polarization features. However, low co-polarization and cross-polarization isolation of 10 dB and 16 dB between WIT and WPT indicate information signal leakage into the rectenna circuit. Moreover, the immediately described works indicated a PCE as high as 70% for high incident RF power ($\geq$ −5 dBm). In contrast the proposed antenna achieves a high PCE of 66.52% at −9.91 dBm input RF power, making it suitable for integration with ultra-low power sensor nodes. The power splitting implemented in [5]–[7] requires integration of directional coupler with the antenna. One of the output ports of the branch line coupler is connected to the rectifier circuit with a matching network and dc low pass filter to achieve rectenna operation. This resulted in larger dimensions of the overall SWIPT system with lower peak isolation (15 dB) and PCE ($\sim$ 50% – 60%) as compared to the proposed design. Furthermore, most of the designs available in the literature have a partial ground structure, thus, resulting in platform dependency where antenna performance varies with the system (sensor node) attached to different platforms. In summary, Table III indicates that the proposed design achieves a high WIT efficiency, high port isolation, and PCE with platform-independent features. Additionally, the integrated DC combining of WPT ports employed in the proposed design realizes full wave rectification and enhances the PCE, which has yet to be explored for designing a SWIPT antenna system.

V. Relevance to Sustainability

The future 6G communication system aims at providing energy efficient and sustainable wireless sensor networks (WSN) [31]. However, the sensor nodes house small batteries limiting the lifespan of WSN. Moreover, the large scale deployment enhances the battery replacement and maintenance cost. Therefore, EH is envisioned as the indispensable technology component of 6G networks for realizing zero-energy wireless sensor nodes to deploy sustainable IoT applications. The WPT technology is perceived as the most suitable choice for EH due to its compact implementation [3]. Moreover, the easy integration of WPT system with the existing RF communication circuitry results in a compact sensor system with SWIPT operation. Moreover, such a system reduces battery waste and helps in realizing the green communication.

VI. Conclusion

In this work, an integrated antenna System with inherent full-wave rectification is proposed to achieve simultaneous wireless information and power transfer (SWIPT) for small IoT sensor nodes. The proposed antenna allows concurrent transmission of wireless information and power transfer (WIT/WPT) using frequency-splitting and dual-polarization techniques. The proposed antenna is a fully integrated design

that eliminates the need for a matching network or dc low-pass filter for rectification. Moreover, the proximity-coupled WIT and capacitive-coupled WPT ports provide high port isolation of ≥ 21.5 dB throughout the WIT operating band (5.7 GHz - 6.0 GHz) and impedes dc backflow into antenna and WIT port. Moreover, the proposed antenna has a smaller size ($0.58\lambda_0 \times 0.53\lambda_0$) than state-of-the-art designs and has a constant WIT efficiency of about $\sim 80\%$ in the entire WIT band with a peak gain of 5.65 dBi at 5.8 GHz. The parallel combining of the dc outputs from the two co-polarized WPT ports realizes highly efficient full-wave rectification (FWR) at an ultra-low input RF power level of -9.91 dBm. The proposed FWR results in a peak PCE of 66.52% with 203.5 mV harvested dc voltage at 610 Ω optimal load. Further, the full ground design realizes platform-independent radiation characteristics. The miniaturized design with high PCE and radiation efficiency makes it suitable for deployment at IoT sensor nodes for sustainable wireless sensor network applications.

REFERENCES

[1] C. D. Alwis, A. Kalla, Q.-V. Pham, P. Kumar, K. Dev, W.-J. Hwang, and M. Liyanage, "Survey on 6G Frontiers: Trends, Applications, Requirements, Technologies and Future Research," *IEEE Open Journal of the Communications Society*, vol. 2, pp. 836–886, 2021.

[2] M. Kumar, S. Kumar, and A. Sharma, "Dual-Purpose Planar Radial-Array of Rectenna Sensors for Orientation Estimation and RF-Energy Harvesting at IoT Nodes," *IEEE Trans. Microw. Wireless Compon. Lett.*, vol. 32, no. 3, pp. 245–248, 2022.

[3] O. L. A. López, H. Alves, R. D. Souza, S. Montejo-Sánchez, E. M. G. Fernández, and M. Latva-Aho, "Massive Wireless Energy Transfer: Enabling Sustainable IoT Toward 6G Era," *IEEE Internet of Things Journal*, vol. 8, no. 11, pp. 8816–8835, 2021.

[4] T. D. Ponnimbaduge Perera, D. N. K. Jayakody, S. K. Sharma, S. Chatzinotas, and J. Li, "Simultaneous Wireless Information and Power Transfer (SWIPT): Recent Advances and Future Challenges," *IEEE Communications Surveys & Tutorials*, vol. 20, no. 1, pp. 264–302, 2018.

[5] P. Lu, K. Huang, C. Song, Y. Ding, and G. Goussetis, "Optimal Power Splitting of Wireless Information and Power Transmission Using a Novel Dual-Channel Rectenna," *IEEE Trans. Antennas Propag.*, vol. 70, no. 3, pp. 1846–1856, 2022.

[6] P. Lu, X.-S. Yang, and B.-Z. Wang, "A Two-Channel Frequency Reconfigurable Rectenna for Microwave Power Transmission and Data Communication," *IEEE Trans. Antennas Propag.*, vol. 65, no. 12, pp. 6976–6985, 2017.

[7] P. Lu, C. Song, and K. M. Huang, "A Two-Port Multipolarization Rectenna With Orthogonal Hybrid Coupler for Simultaneous Wireless Information and Power Transfer (SWIPT)," *IEEE Trans. Antennas Propag.*, vol. 68, no. 10, pp. 6893–6905, 2020.

[8] M. Wagih, G. S. Hilton, A. S. Weddell, and S. Beeby, "2.4 GHz Wearable Textile Antenna/Rectenna for Simultaneous Information and Power Transfer," in *2021 15th European Conference on Antennas and Propagation (EuCAP)*, 2021, pp. 1–5.

[9] L. Liao, Z. Li, Y. Tang, and X. Chen, "Dual-Polarized Dipole Antenna for Wireless Data and Microwave Power Transfer," *Electronics*, vol. 11, no. 5, pp. 1–9, 2022.

[10] M. Wagih, G. S. Hilton, A. S. Weddell, and S. Beeby, "Dual-Band Dual-Mode Textile Antenna/Rectenna for Simultaneous Wireless Information and Power Transfer (SWIPT)," *IEEE Trans. Antennas Propag.*, vol. 69, no. 10, pp. 6322–6332, 2021.

[11] H. K. Sahu and P. R. Sahu, "SSK-Based SWIPT With AF Relay," *IEEE Commun. Lett.*, vol. 23, no. 4, pp. 756–759, 2019.

[12] S. Claessens, N. Pan, D. Schreurs, and S. Pollin, "Multitone FSK Modulation for SWIPT," *IEEE Trans. Microw. Theory Tech.*, vol. 67, no. 5, 2019.

[13] D. Kumar, O. L. Alcaraz López, S. K. Joshi, and A. Tölli, "Latency-Aware Multi-antenna SWIPT System with Battery-Constrained Receivers," *IEEE Trans. Wireless Commun.*, pp. 1–1, 2022.

[14] X.-X. Yang, C. Jiang, A. Z. Elsherbeni, F. Yang, and Y.-Q. Wang, "A Novel Compact Printed Rectenna for Data Communication Systems," *IEEE Trans. Antennas Propag.*, vol. 61, no. 5, pp. 2532–2539, 2013.

[15] M. Ali, G. Yang, and R. Dougal, "A New Circularly Polarized Rectenna for Wireless Power Transmission and Data Communication," *IEEE Antennas Wireless Propag. Lett.*, vol. 4, pp. 205–208, 2005.

[16] M. Wagih, G. S. Hilton, A. S. Weddell, and S. Beeby, "Dual-Polarized Wearable Antenna/Rectenna for Full-Duplex and MIMO Simultaneous Wireless Information and Power Transfer (SWIPT)," *IEEE Open Journal of Antennas and Propagation*, vol. 2, pp. 844–857, 2021.

[17] J.-H. Ou, B. Xu, S. F. Bo, Y. Dong, S.-W. Dong, J. Tang, and X. Y. Zhang, "Highly-Isolated RF Power and Information Receiving System Based on Dual-Band Dual-Circular-Polarized Shared-Aperture Antenna," *IEEE Trans. Circuits Syst. I, Reg. Papers*, vol. 69, no. 8, pp. 3093–3101, 2022.

[18] G.-L. Zhu, J.-X. Du, X.-X. Yang, Y.-G. Zhou, and S. Gao, "Dual-Polarized Communication Rectenna Array for Simultaneous Wireless Information and Power Transmission," *IEEE Access*, vol. 7, pp. 141 978–141 986, 2019.

[19] Y.-M. Zhang and J.-L. Li, "A Dual-Polarized Antenna Array With Enhanced Interport Isolation for Far-Field Wireless Data and Power Transfer," *IEEE Trans. Veh. Technol.*, vol. 67, no. 11, pp. 10 258–10 267, 2018.

[20] H.-M. Lee, "Effect of partial ground plane removal on the front-to-back ratio of a microstrip antenna," in *2013 7th European Conference on Antennas and Propagation (EuCAP)*, 2013, pp. 1204–1208.

[21] B. Clerckx, R. Zhang, R. Schober, D. W. K. Ng, D. I. Kim, and H. V. Poor, "Fundamentals of wireless information and power transfer: From rf energy harvester models to signal and system designs," *IEEE Journal on Selected Areas in Communications*, vol. 37, no. 1, pp. 4–33, 2019.

[22] G. Pabbisetty, K. Murata, K. Taniguchi, T. Mitomo, and H. Mori, "Evaluation of space time beamforming algorithm to realize maintenance-free iot sensors with wireless power transfer system in 5.7-ghz band," *IEEE Transactions on Microwave Theory and Techniques*, vol. 67, no. 12, pp. 5228–5234, 2019.

[23] Y.-X. Sun, K. W. Leung, and K. Lu, "Compact Dual Microwave/Millimeter-Wave Planar Shared-Aperture Antenna for Vehicle-to-Vehicle/5G Communications," *IEEE Trans. Veh. Technol.*, vol. 70, no. 5, pp. 5071–5076, 2021.

[24] M. Kumar, S. Kumar, and A. Sharma, "A Planar Orbicular Rectenna Array System With 3-D Uniform Coverage for Wireless Powering of IoT Nodes," *IEEE Trans. Microw. Theory Tech.*, pp. 1–8, 2022.

[25] T. Matsunaga, E. Nishiyama, and I. Toyoda, "5.8-ghz stacked differential rectenna suitable for large-scale rectenna arrays with dc connection," *IEEE Transactions on Antennas and Propagation*, vol. 63, no. 12, pp. 5944–5949, 2015.

[26] F. Erkmen, T. S. Almoneef, and O. M. Ramahi, "Electromagnetic energy harvesting using full-wave rectification," *IEEE Transactions on Microwave Theory and Techniques*, vol. 65, no. 5, pp. 1843–1851, 2017.

[27] J. McSpadden and K. Chang, "A dual polarized circular patch rectifying antenna at 2.45 ghz for microwave power conversion and detection," in *1994 IEEE MTT-S International Microwave Symposium Digest (Cat. No.94CH3389-4)*, 1994, pp. 1749–1752 vol.3.

[28] P. Lu, C. Song, and K. M. Huang, "A compact rectenna design with wide input power range for wireless power transfer," *IEEE Trans. Power Electron.*, vol. 35, no. 7, pp. 6705–6710, 2020.

[29] M. Kumar, S. Kumar, S. Jain, and A. Sharma, "A Plug-in Type Integrated Rectenna Cell for Scalable RF Battery Using Wireless Energy Harvesting System," *IEEE Microwave and Wireless Technology Letters*, vol. 33, no. 1, pp. 98–101, 2023.

[30] R. Trevisoli, H. P. d. Paz, V. S. d. Silva, R. T. Doria, I. R. S. Casella, and C. E. Capovilla, "Modeling Schottky Diode Rectifiers Considering the Reverse Conduction for RF Wireless Power Transfer," *IEEE Trans. Circuits Syst. II, Exp. Briefs*, vol. 69, no. 3, pp. 1732–1736, 2022.

[31] A. A. Benbuk, N. Kouzayha, J. Costantine, and Z. Dawy, "Charging and Wake-Up of IoT Devices using Harvested RF Energy with Near-Zero Power Consumption," *IEEE Internet of Things Magazine*, vol. 6, no. 1, pp. 162–167, 2023.